Articles

Encapsulated $HRh(CO)(PPh_3)_3$ in Microporous and Mesoporous Supports: Novel Heterogeneous Catalysts for Hydroformylation

Kausik Mukhopadhyay,[†] Anand B. Mandale,[‡] and Raghunath V. Chaudhari*[,†]

Homogeneous Catalysis Division and Physical Chemistry (SIL) Division, National Chemical Laboratory, Pune 411008, India

Received July 24, 2002. Revised Manuscript Received December 16, 2002

Novel heterogeneous catalysts for hydroformylation of olefins to aldehydes using encapsulation and anchoring methodologies for $HRh(CO)(PPh_3)_3$ in zeolite Na−Y and MCM-41 and MCM-48 mesoporous materials have been reported. The heterogeneous catalysts were characterized and used for hydroformylation of linear and branched olefins to show high activity and recyclability without leaching of the Rh metal during the course of reactions. Using CP-MAS NMR, FT-IR, TEM, XPS, and powder XRD studies, characterization of the Rh complex inside the porous structures of the heterogeneous catalysts has been investigated. ^{31}P CP-MAS NMR spectra of the encapsulated Rh complex catalyst inside zeolite Na−Y and mesoporous MCM-41 and MCM-48 supports showed a possible encapsulation of the Rh complex in the pores. TEM images and the diffraction patterns of the heterogenized Rh complex in mesoporous and zeolitic supports further supported a possible entrapment of the complex inside the porous frameworks. Rhodium is present as Rh(I) in the encapsulated catalysts before and after the experiments, as envisaged by XPS spectra. In contrast to other heterogeneous catalytic systems for hydroformylation, the catalysts reported here are highly stable, easily separable, and recyclable. The TON/TOF values of these catalysts were also found to be significantly higher than those of the previously reported heterogeneous catalysts.

Introduction

Homogeneous catalysis is gaining considerable interest due to its high activity and selectivity at milder reaction conditions for a wide variety of reactions.[1] However, their practical applications have been limited by difficulties in achieving industrially viable catalyst−product separation.[2] In this context, encapsulation of metal complexes as a means of "heterogenization" has particular significance. Zeolites and zeotypes (molecular sieves), owing to their varied intrinsic properties (e.g., acidity, basicity, redox behavior, etc.), channel sizes, high surface areas, thermal and chemical stabilities, and channel structures (shape selectivities), have been extensively used in oil refining, petrochemical, and fine chemical industries for the past couple of decades.[3] But the limitation of pore sizes (less than 13 Å) of these microporous materials demanded a search for new materials with larger pore sizes. The exploration resulted in the discovery of a novel family of mesoporous materials called M41S that opened new opportunities in catalytic applications.[4] The M41S family has been generally classified into three different categories: MCM-41 (hexagonal), MCM-48 (cubic), and MCM-50 (lamellar).[5] The properties of the mesoporous materials such as larger surface areas (>700 m^2g^{-1}), well-defined pore sizes (20−100 Å), and tenability to change the pore sizes have made them the most sought after materials of the past decade. The syntheses of these materials with the aid of host−guest chemistry have expanded the applica-

* Corresponding author. E-mail: rvc@ems.ncl.res.in. Fax: 0091-20-5893260.

[†] Homogeneous Catalysis Division.

[‡] Physical Chemistry (SIL) Division.

(1) Parshall, G. W.; Ittel, S. D. *Homogeneous Catalysis*; John Wiley & Sons: New York, 1992.

(2) (a) Hartley, F. R. *Supported Metal Complexes*; Reidel: Dordrecht, The Netherlands, 1985. (b) Beller, M., Bolm, C., Eds. *Transition Metals for Organic Synthesis*; Wiley-VCH: Weinheim, 1998; Vol. 2, Chapters 1 & 2. (c) Herrmann, W. A.; Cornils, B. *Angew. Chem., Intl. Ed. Engl.* **1997**, *36*, 1048. (d) Bailey, D. C.; Langer, S. H. *Chem. Rev.* **1981**, *81*, 109.

(3) (a) Breck, D. W. *Zeolite Molecular Sieves: Structure, Chemistry and Uses*; Wiley: New York, 1974. (b) Corma, A. *Chem. Rev.* **1995**, *95*, 559. (c) Corma, A. *Chem. Rev.* **1997**, *97*, 2373.

(4) De Vos, D. E.; Dams, M.; Sels, B. F.; Jacobs, P. A. *Chem. Rev.* **2002**, *102*, 3615.

(5) (a) Kresge, C. T.; Leonowicz, M. E.; Roth, W. J.; Vertulli, J. C.; Beck, J. S. *Nature* **1992**, *359*, 710. (b) Beck, J. S.; Vertulli, J. C.; Roth, W. J.; Leonowicz, M. E.; Kresge, C. T.; Schmitt, K. D.; Chu, C. T.-W.; Olson, D. H.; Sheppard, E. W.; McCullen, S. B.; Higgins, J. B.; Schlenker, J. L. *J. Am. Chem. Soc.* **1992**, *114*, 10834. (c) Monnier, A.; Schuth, F.; Huo, Q.; Kumar, D.; Margolese, D.; Maxwell, R. S.; Stucky, G. D.; Krishnamurthy, M.; Petroff, P.; Firouzi, A.; Janicke, M.; Chmelka, B. F. *Science* **1993**, *261*, 1299.

10.1021/cm020752n CCC: $25.00
Published on Web 04/04/2003

Scheme 1. Hydroformylation of Olefins Using $HRh(CO)(PPh_3)_3$ Encapsulated Catalysts

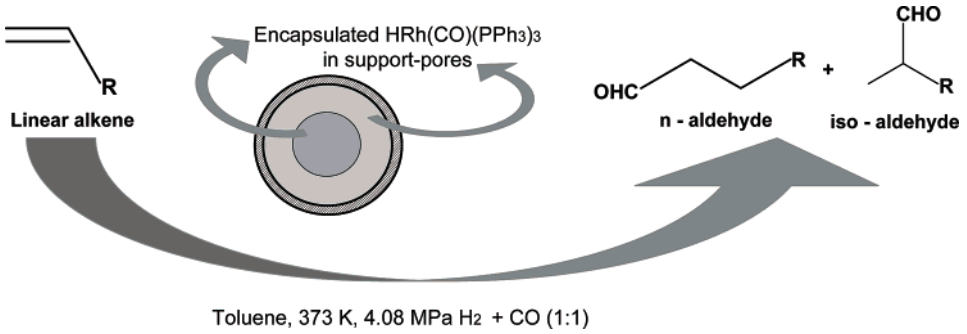

tions of solid catalysts for developing new processes for fine and bulk chemicals. In the immobilization approach, the organometallic complex is encapsulated or anchored inside the pores of the inorganic inert matrixes (e.g., zeolites, M41S materials, clay, etc.) in such a way that the complex is tightly bound inside the pores.[6] The prime requirement is stability of the encapsulated complex, so that it does not leach out of the catalyst pores to the liquid phase in the course of a reaction, while retaining high activity, selectivity, and original configuration. In several reports, heterogeneous catalysis by encapsulated supports has been addressed for carbonylation, oxidation, hydrogenation, epoxidation, and Heck reactions,[7] but attempts to heterogenize some of the industrially relevant homogeneous catalysts have been very limited.

Hydroformylation is one of the largest scale applications of homogeneous catalysis in industry.[8] In previous work, polymer-anchored, supported liquid phase (SLP), supported aqueous phase (SAP), biphasic catalysts using water-soluble metal complexes using sulfonated or fluorinated phosphines as ligands, as well as bimetallic catalysts for hydroformylation have been proposed.[9] In these reports, interesting concepts have emerged; however, with the exception of biphasic catalysis no other approach has been found to be commercially attractive. Even the biphasic catalysts for hydroformylation of higher olefins suffer from the disadvantages of the lower rates limited by the solubility of olefins in water. To overcome the separation problems, several immobilized catalysts were reported earlier,[10] but these unfortunately suffer either from lower selectivity and activity (TON), or low recyclability, or use expensive ligands, and hence, are not suitable for practical applications. We report here synthesis, characterization, and catalytic efficiency of encapsulated $HRh(CO)(PPh_3)_3$ in microporous Na−Y (Si/Al = 2.37), and mesoporous Si−MCM-41 and Si−MCM-48 supports as catalysts for hydroformylation of olefins (Scheme 1) with excellent recyclability. These catalysts also function without using excess PPh_3 ligand as often required in homogeneous catalytic reactions.

Experimental Section

1. Materials. The materials required for zeolite Na−Y were sodium silicate (Loba, India) as silica source, sodium aluminate ($NaAlO_2$) and aluminum sulfate ($Al_2(SO_4)_3 \cdot 16H_2O$) as aluminum sources, and sodium hydroxide (all procured from s. d. Fine Chem, India). In the syntheses of MCM-41 and MCM-48 materials, fumed SiO_2 (380 m^2g^{-1}, Aldrich) as a silica source, cetyl trimethylammonium bromide (CTABr, Aldrich) as a template, and dodecaphosphotungstic acid (PTA, Aldrich) as a promoter to accelerate the syntheses, were used. Deionized water was used throughout the syntheses of zeolite Y and mesoporous materials. Rhodium chloride ($RhCl_3 \cdot 3H_2O$, 40% Rh, Aldrich), sodium borohydride ($NaBH_4$, s. d. Fine Chem), triphenyl phosphine (PPh_3, Aldrich), ethanol (EtOH, 99.9%, BDH, UK), and formaldehyde solution (37% HCHO, s. d. Fine Chem) were used for the synthesis of $HRh(CO)(PPh_3)_3$ complex.

2. Synthesis. *(a) Zeolite Na−Y and Encapsulated Wilkinson's Complex $HRh(CO)(PPh_3)_3$ in Na−Y.* In a typical synthesis of zeolite Na−Y, seed crystals of zeolite Na−Y were prepared separately from an aqueous mixture of Na_2SiO_3 (95 mmol, 28% SiO_2 and 8.4% Na_2O), $NaAlO_2$ (9.76 mmol, 43% Al_2O_3, 39% Na_2O), NaOH (70 mmol), and 10 mL of H_2O by stirring for 1 h and keeping it at rest for 18 h. The seed crystals of zeolite Na−Y thus prepared were then added to an aqueous solution of Na_2SiO_3 (355 mmol). Subsequent addition of $NaAlO_2$ (34.2 mmol), NaOH (92.5 mmol), $Al_2(SO_4)_3 \cdot 16H_2O$ (6.02 mmol), and 35 mL of H_2O was followed under constant stirring for 2 h. The overall initial gel composition of the zeolite Na−Y was

(6) (a) Bein, T. *Compr. Supramol. Chem.* **1996**, *7*, 579. (b) Shephard, D. S.; Zhou, W.; Maschmeyer, T.; Matters, J. W.; Roper, C. L.; Parsons, S.; Johnson, B. F. G.; Duer, M. J. *Angew. Chem., Int. Ed.* **1998**, *37*, 2719. (c) Ertl, G., Knoezinger, H., Weitkamp, J., Eds. *Handbook of Heterogeneous Catalysis*; Wiley-VCH: Weinheim, 1997.

(7) (a) Mukhopadhyay, K.; Sarkar, B. R.; Chaudhari, R. V. *J. Am. Chem. Soc.* **2002**, *124*, 9692. (b) Gerrits, P. P. K.; De Vos, D. E.; Starzyk, F. T.; Jacobs, P. A. *Nature* **1994**, *369*, 543. (c) Raja, R.; Ratnasamy, P. *J. Mol. Catal.* **1995**, *100*, 93. (d) Corma, A.; Nemeth, L. T.; Renz, M.; Valencia, S. *Nature* **2001**, *412*, 423. (e) Kowalak, S.; Weiss, R. C.; Balkus, K. J., Jr. *J. Chem. Soc. Chem. Commun.* **1991**, 57. (f) Ogunwumi, S. B.; Bein, T. *Chem. Commun.* **1997**, 901. (g) Mehnert, C. P.; Weaver, D. W.; Ying, J. Y. *J. Am. Chem. Soc.* **1998**, *120*, 12289. (h) Djakovitch, L.; Koehler, K. *J. Am. Chem. Soc.* **2001**, *123*, 5990.

(8) (a) Falbe, J. *Carbon Monoxide in Organic Synthesis*, Springer-Verlag: Berlin/Heidelberg, 1970. (b) Cornils, B., Hermann, W. A., Eds. *Applied Homogeneous Catalysis with Organometallic Compounds*; VCH: Weinheim, 1996; Volumes 1 and 2.

(9) (a) Pittmann, C. U., Jr.; Smith, L. R. *J. Am. Chem. Soc.* **1975**, *97*, 1742. (b) Rony, P. R. *J. Catal.* **1969**, *14*, 142. (c) Arhancet, J. P.; Davis, M. E.; Merola, J. S.; Hanson, B. E. *Nature* **1989**, *339*, 554. (d) Kuntz, E. *CHEMTECH* **1987**, *17*, 570. (e) Hermann, W. A.; Albanese, G. P.; Manetsberger, R. B.; Lappe, P.; Bahrmann, H. *Angew. Chem., Intl. Ed. Engl.* **1995**, *34*, 811. (f) Horvarth, I. T.; Rabai, J. *Science* **1994**, *266*, 72. (g) Broussard, M. E.; Juma, B.; Train, S. G.; Peng, W.-J.; Laneman, S. A.; Stanley, G. G. *Science* **1993**, *260*, 1784. (h) Nowotny, M.; Maschmeyer, T.; Johnson, B. F. G.; Lahuerta, P.; Thomas, J. M.; Davies, J. E. *Angew. Chem., Int. Ed.* **2001**, *40*, 955. (i) Mecking, S. Thomann, R. *Adv. Mater.* **2000**, *12*, 953. (j) Rojas, S.; M-Mascaros, S.; Terreros, P.; Fierro, J. L. G. *New J. Chem.* **2001**, *25*, 1430.

(10) (a) Andersen, J. M.; Currie, A. W. S. *Chem. Commun.* **1996**, 1543. (b) Davis, M. E.; Butler, P. M.; Rossin, J. A. *J. Mol. Catal.* **1985**, *31*, 385. (c) Bourque, S. C.; Alper, H. *J. Am. Chem. Soc.* **2000**, *122*, 956. (d) Shimizu, S.; Shirakawa, S.; Sasaki, Y.; Hirai, C. *Angew. Chem., Int. Ed.* **2000**, *39*, 1256. (e) Sandee, A. J.; van der Veen, L. A.; Reek, J. N. H.; Kamer, P. C. J.; Lutz, M.; Spek, A. L.; van Leeuwen, P. W. N. M. *Angew. Chem., Int. Ed.* **1999**, *38*, 3231. (f) Meehan, N. J.; Sandee, A. J.; Reek, J. N. H.; Kamer, P. C. J.; van Leeuwen, P. W. N. M.; Poliakoff, M. *Chem. Commun.* **2000**, 1497. (g) Bianchini, C.; Burnaby, D. G.; Evans, J.; Frediani, P.; Meli, A.; Oberhauser, W.; Psaro, R.; Sordelli, L.; Vizza, F. *J. Am. Chem. Soc.* **1999**, *121*, 5961. (h) Mukhopadhyay, K.; Nair V. S.; Chaudhari, R. V. *Stud. Surf. Sci. Catal.* **2000**, *130*, 2999.

Table 1. Physical Characteristics of the Supports and the Encapsulated Catalysts[21]

material	Rh (wt %)	d_{hkl} (Å)[a]	a_o (Å)[b]	surface area ($m^2\ g^{-1}$)	particle size (μm)	ν (cm^{-1})[c]	(Q^3/Q^4)[d]
Na−Y		14.29 (111)	24.75	735	0.5 × 0.7		
Wk−Y−S	0.567	14.43 (111)	24.99	n.d.	0.5 × 0.7	n.d.	
Wk−Y	1.130	14.48 (111)	25.08	n.d.	0.55 × 0.8	1930, 513	
MCM-41		41.63 (100)	48.07	1251	0.75 × 2.0		1.2 (0.32)
Wk-M41	0.747	41.83 (100)	48.30	n.d.	0.75 × 2.0	1965, 517	0.05
MCM-48		36.93 (211)	90.46	1682	0.5 × 1.0		0.8 (0.18)
Wk-M48	0.690	37.09 (211)	90.85	n.d.	0.5 × 1.0	1966, 518	0.05
$HRh(CO)(PPh_3)_3$	11.21					1922, 514	

[a] Calculated from powder XRD spectra ($n\lambda = 2d\sin\theta$; $n = 1$, $\lambda = 1.5404$ Å), values in parentheses are respective, principal Bragg reflections. [b] Determined by: $a_o = d_{111} \times \sqrt{3}$ (zeolite Y supports); $a_o = d_{100} \times 2/\sqrt{3}$ (MCM-41 supports); $a_o = d_{211} \times \sqrt{6}$ (MCM-48 supports). [c] Transmittance FT-IR spectra, 'ν' values (from left to right) are for Rh−CO and Rh−P bands (see refs 14c, d). [d] As-synthesized samples, values in parentheses are for calcined samples; n. d. = not determined.

$SiO_2/Al_2O_3/Na_2O/H_2O$ (5.05:1:5.46:111.58). $HRh(CO)(PPh_3)_3$, prepared as reported earlier by Evans et al.,[11] (∼0.135 mmol) was then dissolved in 30 mL of EtOH, and the solution was finally added to the zeolite Na−Y gel under stirring for 1 h; pH of the final gel was 13.1. The choice of ethanol as the solvent was made considering its complete miscibility with water, and hence, also with the ethanolic solution of the Rh complex in the aqueous gel of the zeolite. The mixture of $HRh(CO)(PPh_3)_3$−zeolite gel was then sealed in a polypropylene bottle and kept in an oven at 373 K for 12 h under autogenous pressure. The samples were then filtered and washed several times with de-ionized water, dried at 353 K, and Soxhlet-washed twice with dry toluene to ensure that no free complex was adhered to the encapsulated zeolite (sample labeled as **Wk−Y**).

Henceforth, we have labeled all the encapsulated catalysts by the term "**Wk**" as an abbreviation for the Wilkinson's catalyst/complex, $HRh(CO(PPh_3)_3$.

(b) Supported $HRh(CO)(PPh_3)_3$ on Zeolite Na−Y (by Impregnation). Supported $HRh(CO)(PPh_3)_3$ on zeolite Na−Y was prepared by suspending 3 g of Na−Y in ethanolic solution containing 0.135 mol of the complex and refluxing it at 363 K for 18 h. The light yellow solid was filtered and dried at 353 K and used as such (labeled as **Wk−Y−S**) for analysis by ^{31}P CP-MAS NMR spectra and hydroformylation reactions.

(c) Synthesis of Si−MCM-41 and Si−MCM-48. Following a procedure reported earlier,[12] Si−MCM-41 and Si−MCM-48 were synthesized having initial gel compositions of SiO_2/NaOH/CTABr/H_2O/PTA (1:0.32:0.2:125:0.0033) and SiO_2/NaOH/CTABr/H_2O/PTA (1:0.4:0.21:120:0.0033), respectively (PTA = phosphotungstic acid). In a typical synthesis of MCM-41, 50 mmol fumed SiO_2 was added to a solution of 16 mmol NaOH in 25 mL of H_2O and stirred for 1 h. To this mixture, 10 mmol CTABr is added dropwise followed by an addition of 0.165 mmol PTA (as a promoter) in 37 mL of H_2O. The final gel was stirred for another 1.5 h and then autoclaved in a polypropylene bottle at 373 K for 4 h. The as-synthesized sample was then filtered, washed repeatedly with deionized water, and air calcined at 813 K to obtain calcined Si−MCM-41.

In the synthesis of MCM-48, 50 mmol fumed silica was added to a solution of 20 mmol NaOH in 25 mL of H_2O and stirred for 1 h. To this mixture, 10.5 mmol of CTABr was added dropwise followed by an addition of 0.165 mmol PTA (as a promoter) in 33 mL of H_2O. The final gel was stirred for another 1.5 h and then autoclaved in a Teflon-lined stainless steel autoclave at 423 K for 12 h. The as-synthesized sample was then filtered, washed repeatedly with deionized water, and air calcined at 813 K to obtain calcined Si−MCM-48.

(d) Functionalization of Si−MCM-41 and Si−MCM-48 by APTS and Anchoring of $HRh(CO)(PPh_3)_3$ Complex Inside the Mesopores. Functionalization of Si−MCM-41 and Si−MCM-48 was done by a procedure reported earlier by Mukhopadhyay et al.[7a] A 1.0-g aliquot of Si−MCM-41 or Si−MCM-48 was suspended in 30 mL of dry dichloromethane (DCM). To this 0.142 mmol dichlorodiphenylsilane (Ph_2SiCl_2, Fluka) was added, and the mixture was stirred for 1 h. The contents were then cooled to 195 K, and 5.73 mmol 3-aminopropyltrimethoxysilane (APTS, Aldrich) was added dropwise to this slurry, which was stirred for a further 24 h at 313 K. The contents were filtered, washed repeatedly with dry DCM, and dried in a vacuum to get functionalized MCM-41 and MCM-48 supports.

To prepare the anchored $HRh(CO)(PPh_3)_3$ catalysts in MCM-41 and MCM-48, 1.0 g of the functionalized support (MCM-41 or MCM-48) was added to a solution containing the Rh complex (∼0.108 mmol) in 100 mL of dry, distilled ethanol and stirred for 16 h at room temperature. The light yellow solid powder was then washed several times with dry ethanol, Soxhlet-extracted once with EtOH to remove any Rh complex adhered to the support walls, then dried and stored under vacuum. The catalysts thus prepared (labeled as **Wk-M41** and **Wk-M48**), were used as such for hydroformylation reactions. Some important physical characteristics of all three encapsulated catalysts are presented in Table 1.

In a similar fashion, we also prepared $HRh(CO)(PPh_3)_3$ tethered to the external surfaces of APTS grafted MCM-41 and MCM-48 without Ph_2SiCl_2 treatment (labeled as **Wk-M41−S** and **Wk-M48−S**). These materials were used for comparison of the TEM images and hydroformylation reaction data (especially to compare the TEM patterns for Rh complex grafted on/in the supports and Rh leaching in the reaction mixture using **Wk-M48−S**) with those of the encapsulated catalysts (**Wk-M41** and **Wk-M48**). The comparisons have been discussed in detail in later sections of the text. For the sake of simplicity, the word "encapsulated" has been used throughout the text in the case of $HRh(CO)(PPh_3)_3$ anchored to the amine-functionalized mesoporous supports.

This unique approach of passivation of the external-surface silanol groups (Si−OH) of the mesoporous materials by reacting with controlled amount of Ph_2SiCl_2 and subsequent treatment with APTS for selective functionalization of the inner-surface Si−OH groups of the mesoporous matrixes was reported earlier by Shephard et al.[6b] The silylation reaction between Ph_2SiCl_2 and the external-surface Si−OH groups deactivated the silanol groups. Thus, the treatment of Ph_2SiCl_2 with the mesoporous materials compelled anchoring of APTS as well as Rh complex selectively inside the mesopore channels.

3. Hydroformylation Reaction Setup. All the hydroformylation reactions were carried out in a 50-mL reactor (Parr Instrument Company, Moline, IL) at 373 K and 4.08 MPa of 1:1 CO + H_2, using toluene as a solvent. In a typical experiment, a known amount of olefin with degassed toluene and heterogenized catalyst were charged into the reactor and the contents were flushed with nitrogen and then with a mixture of 1:1 CO and H_2. The contents of the reactor were heated to a desired temperature, and then a mixture of CO and H_2 (1:1) from a pre-filled reservoir vessel (maintained at higher pressure than the reactor) was introduced slowly into the autoclave up to a desired pressure. A sample of the liquid

(11) Evans, D.; Osborn, J. A.; Wilkinson, G. J. *J. Chem. Soc. A.* **1968**, 3133.
(12) Mukhopadhyay, K.; Ghosh, A.; Kumar, R. *Chem. Commun.* **2002**, 2404.

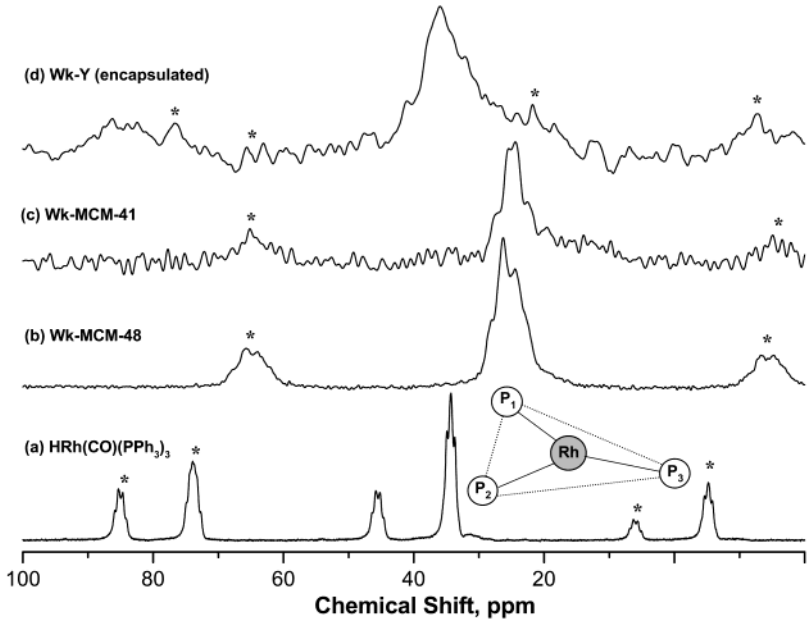

Figure 1. ^{31}P CP-MAS NMR spectra of different catalysts (inset of (a): trigonal plane of $HRh(CO)(PPh_3)_3$ comprising three phosphorus atoms (designated as P_1, P_2, and P_3) bonded to Rh atom, atoms are not to scale; * in NMR patterns denote sidebands at 8 kHz).

phase mixture was withdrawn and the reaction was started by switching the stirrer on. The reaction was then continued at a constant pressure of CO and H_2 by supplying CO/H_2 mixture as per consumption from the reservoir vessel using a constant pressure regulator.

Safety Note: Hydroformylation experiments should be performed with utmost care and precautions as they involve use of CO and H_2 at high pressures.

4. Leaching and Recycle Experiments with the Heterogeneous Catalysts. Catalyst leaching experiments have been performed by hot filtration of the reaction mixture at 373 K and subsequently testing the catalytic activity of the filtrates for hydroformylation without addition of catalyst. These solutions and the catalysts thus recovered were also analyzed for determination of Rh content by inductively coupled plasma with atomic emission spectra (ICP-AES) analyses. In a typical catalyst recycle experiment, the heterogeneous catalyst was allowed to settle down and the clear supernatant liquid was decanted slowly. The residual solid catalyst was reused with fresh charge of solvent and reactants for further recycle runs maintaining the same reaction conditions. In the recycle studies, the rhodium content of the catalyst and subsequent hydroformylation reaction mixtures were analyzed for metal content as well as metal leaching.

Results and Discussion

1. Characterization of Catalysts. The catalysts were characterized using ^{31}P CP-MAS NMR, ^{29}Si and ^{27}Al MAS NMR, FT-IR spectroscopy, X-ray photoelectron spectra, powder X-ray diffraction, and transmission electron microscopy.

(a) ^{31}P CP-MAS NMR Spectra of $HRh(CO)(PPh_3)_3$. ^{31}P CP-MAS (cross-polarized, magic angle spinning) NMR spectra of $HRh(CO)(PPh_3)_3$ complex and the Rh complex inside the pores of Na−Y, MCM-41, and MCM-48 materials (shown in Figure 1) were obtained on a Bruker DRX 500 FT-NMR spectrometer at 202.64 MHz and 11.7 T using a 3-mm CP-MAS probe. The chemical shifts were referred to H_3PO_4 at 0 ppm and the spectra were collected at a spectral width of 20 kHz, with a flip angle of 45°, 6000 real data points, and 5-s relaxation delay.

A coupled ^{1}H−^{31}P CP-MAS NMR spectra of the pure $HRh(CO)(PPh_3)_3$ complex shows two major ^{31}P peaks ($\delta_{iso} = 34.4$, 45.4 ppm), each split by J coupling to other ^{31}P and ^{103}Rh ($n = 100\%$) nuclei (Figure 1a). Considering the dipolar and anisotropic part of the J couplings are averaged to zero by magic angle spinning, the observed multiplet structure arises due to the isotropic P−P and P−Rh scalar couplings.[13a] We observed that the chemical shift difference for the two major signals ($\delta_{iso} = 34.4$, 45.4 ppm) is larger than the P−P scalar couplings and the integrated intensity for these major signals is in the ratio of 2:1. The three phosphorus atoms in the $HRh(CO)(PPh_3)_3$ complex may be grouped into one distinct (P_3) and two equivalent (P_1 and P_2) environments (inset of Figure 1a). For the distinct P_3 atom, the coupling to two equivalent phosphorus (P_1 and P_2) nuclei by P−P coupling ($J_{P-P} = 127.5$ Hz) and to rhodium by P−Rh coupling ($J_{P-Rh} = 142.3$ and 140.6 Hz) causes the observed multiplet in the intensity ratio of 1:3:3:1. Similarly, the equivalent P_1− P_2 atoms are split into a doublet by the distant P_3 atom, further split by coupling to rhodium to give a doublet of a doublet. However, because $|J_{P-P} - J_{P-Rh}| < \Delta\nu$ ($\Delta\nu$ is the MAS line width), we observe only a triplet. On the basis of the observed J_{P-P} values, the three phosphorus atoms are expected to be in a plane with P−Rh−P angle ∼120°, which leads to a structure with least strain from the three bulky PPh_3 groups. Due to random orientations of the nine phenyl groups in the Rh complex, all the atoms in the molecule become crystallographically nonequivalent, as

(13) For an excellent discussion on ^{31}P CP-MAS of $HRh(CO)(PPh_3)_3$ complex, see (a) Wu, G.; Wasylishen, R. E.; Curtis, R. D. *Can. J. Chem.* **1992**, *70*, 863. (b) Diesveld, J. W.; Menger, E. M.; Edzes, H. T.; Veeman, W. S. *J. Am. Chem. Soc.* **1980**, *102*, 7936. (c) Wu, G.; Wasylishen, R. E. *Organometallics* **1992**, *11*, 3242. For discussions on ^{31}P CP-MAS of rhodium−phosphine complexes on silica-type supports, see (d) Lindner, E.; Schneller, F.; Auer, F.; Mayer, H. A. *Angew. Chem., Int. Ed.* **1999**, *38*, 8, 2154, and references therein. (e) Scott, S. L.; Szpakowicz, M.; Mills, A.; Santini, C. C. *J. Am. Chem. Soc.* **1998**, *120*, 1883.

also noticed by the X-ray crystal structure.[14a,b]

Assignments for the three phosphorus atoms (P_1, P_2, P_3) can be made based on the P−Rh−CO bond angle,[14a−c] which shows a larger difference than compared to the P−Rh bond distances. Compared to the P_1 and P_2 atoms, the P_3 atom has a larger bond angle that results in a better overlap of the bonding orbital; hence, the electronegative effect of CO would be felt more on the P_3 atom to cause a downfield shift, which we indeed observe. Thus, the P_3 atom can be assigned to the low-field multiplet; and P_1 and P_2 atoms can be assigned as the high-field triplets in our observed spectra. The ^{31}P CP-MAS results clearly show that $HRh(CO)(PPh_3)_3$ complex has a distorted trigonal bipyramidal (TBP) structure (local symmetry tends toward C_s instead of C_{3v}) in which the three phosphorus atoms lie in the basal plane (this is in perfect agreement with the spectral analysis[13a] and crystal structure[14a] reported earlier).

(b) ^{31}P CP-MAS NMR and FT-IR Spectra of the Encapsulated Catalysts. To validate that the $HRh(CO)(PPh_3)_3$ complex was encapsulated in zeolite Na−Y, mesoporous MCM-41, and MCM-48 materials, solid-state ^{31}P CP-MAS NMR spectra of the encapsulated catalyst (Wk−Y, Wk-M41, and Wk-M48) were recorded and compared with the spectra obtained for $HRh(CO)(PPh_3)_3$.

The ^{31}P CP-MAS spectra of Wk-M41 and Wk-M48 samples (Figure 1b and c) showed a marked difference in chemical shifts when compared with the Rh complex. The upfield shifts for Wk-M41 ($\delta_{iso} = 25.4$ ppm) and Wk-M48 ($\delta_{iso} = 26.0$ ppm) in comparison to that observed for the Rh complex ($\delta_{iso} = 34.4$, 45.4 ppm) for these two materials suggests that there is a definite coordination between N_{APTS} and the Rh atom. APTS (anchored inside the mesopores' walls of MCM-41 and MCM-48), when bound with the Rh complex, donates the electron pair from N_{APTS} to the Rh atom (Figure 6a), which in turn increases the electron density on the P_{PPh3} atoms (of the complex) by a $(d\pi)_P-(d\pi)_{Rh}$ bonding, a fact that we observed earlier for anchored Pd−phosphine complex in mesoporous systems.[7a] It was indiscernible to classify the ^{31}P splitting for Wk-M48 or Wk-M41 based on J coupling since the splitting, as well as the line broadening, was much larger than the J_{P-P} or J_{P-Rh} observed for the Rh complex. This may be due to either (1) the change in geometry from the distorted TBP structure of $HRh(CO)(PPh_3)_3$ to an octahedral one due to coordination of the N_{APTS} and Rh atoms, or (2) loss of a PPh_3 atom from the complex while anchoring in the mesopores' walls. The possibility of having two resonances in 1:2 ratio similar to that of the neat Rh complex is unlikely even if there are three PPh_3 groups attached to the Rh atom, since crystallographic nonequivalence and retention of the original structure of Rh complex anchored inside the mesopores' walls is no longer viable.[13b] The fact that we did not observe any spectral line for free PPh_3 ligand in the filtrate solutions after filtration of the solid catalysts ($\delta_{iso} = -3.5$ ppm by ^{31}P−$CDCl_3$ spectra) indicates that coordination of the Rh complex with the APTS-tethered MCM materials does not proceed through cleavage of a PPh_3 ligand from the Rh complex (a fact well-known for the dissociation of the Rh complex in solution and hydroformylation reactions). This further strengthens our presumption based on the change in geometry due to N_{APTS}−Rh complex coordination. In case of subsequent loss of one PPh_3 atom and addition of one N_{APTS} atom to Rh, we would have obtained spectra similar to that of bis(triphenylphosphine) rhodium complex.[13b−e] In contrast, we see quite different spectra for the encapsulated Wk-M41 and Wk-M48 catalysts wherein the broad spectral line appears at one place with a complex splitting pattern. In this context, we refer to a report by Lindner et al.[13d] wherein it has been shown that ^{31}P CP-MAS spectra of the Rh−triphosphanyl complex bound to a polysiloxane matrix gives rise to a broad spectral line with complex patterns, similar to the spectral patterns we have obtained. The Rh−phosphanyl complex attached inside the polymer matrix has an octahedral geometry, which is similar to the Rh complex bound to Wk-M41 and Wk-M48 catalysts. Thus, on the basis of the inferences obtained herein, a plausible reason for the absence of the Rh complex multiplet peak ushers $HRh(CO)(PPh_3)_3$ anchored inside the mesopores of MCM-41 and MCM-48 with a change in geometry from TBP to octahedral.

Interestingly, the ^{1}H−^{31}P CP-MAS NMR spectrum of catalyst Wk−Y (Figure 1d) showed a different pattern in chemical shift ($\delta_{iso} = 36.1$, 47.1 ppm; signal-to-noise ratio was poor for this sample, hence a weak spectral line is observed at 47.1 ppm). The changes in signal positions indicate a geometrical constraint in Wk−Y. To further ensure that the Rh complex is encapsulated inside the faujasite supercage in case of Wk−Y, a ^{31}P MAS experiment was performed for the Wk−Y−S sample. ^{31}P MAS spectrum of Wk−Y−S was taken in the Bloch decay mode with proton decoupling, because no ^{1}H−^{31}P cross-polarization MAS spectrum for this sample was feasible, presumably because of high surface mobility of the physisorbed or chemisorbed species. Despite the somewhat poor spectra/noise for Wk−Y−S sample, a comparison of ^{31}P CP-MAS spectra of samples $HRh(CO)(PPh_3)_3$ and Wk−Y−S (spectra not shown) clearly show that the two major ^{31}P signals ($\delta_{iso} = 34.4$, 45.8 ppm) are observed at nearly the same chemical shifts. A mere surface adsorption, rather than encapsulation, is envisaged in the case of Wk−Y−S catalyst that consists of $HRh(CO)(PPh_3)_3$ impregnated on zeolite Na−Y. Both these observations suggest that in case of Wk−Y, a possible encapsulation of $HRh(CO)(PPh_3)_3$ in the supercage of Na−Y zeolite has occurred.

Infrared (Fourier transform) transmittance spectra were performed on a Bio-Rad instrument for detecting the Rh−CO and Rh−P bands[14c,d] of the Rh complex and the encapsulated catalysts (Table 1). FT-IR spectra of the Rh complex (1922 cm^{-1}, 514 cm^{-1}) and Wk−Y catalyst (1930 cm^{-1}, 513 cm^{-1}) revealed almost similar ν_{Rh-CO} and ν_{Rh-P} respectively. In contrast, Wk-M41 and Wk-M48 catalysts showed distinguishable ν_{Rh-CO} and ν_{Rh-P} bands at 1965 $cm^{-1}$and 518 cm^{-1} respectively; an increase in electron density on the Rh−CO and Rh−P due to N_{APTS}−Rh coordination might be a plausible reason for this change. Broad bands at 3430 cm^{-1} were also observed in the IR spectra of these two catalysts,

(14) (a) La Placa, S. J.; Ibers, J. A. *J. Am. Chem. Soc.* **1963**, *85*, 3501. (b) La Placa, S. J.; Ibers, J. A. *Acta Crystallogr.* **1965**, *18*, 511. (c) Bath, S. S.; Vaska, L. *J. Am. Chem. Soc.* **1963**, *85*, 3500. (d) Janssen, A.; Niederer, J. P. M.; Holderich, W. F. *Catal. Lett.* **1997**, *48*, 165.

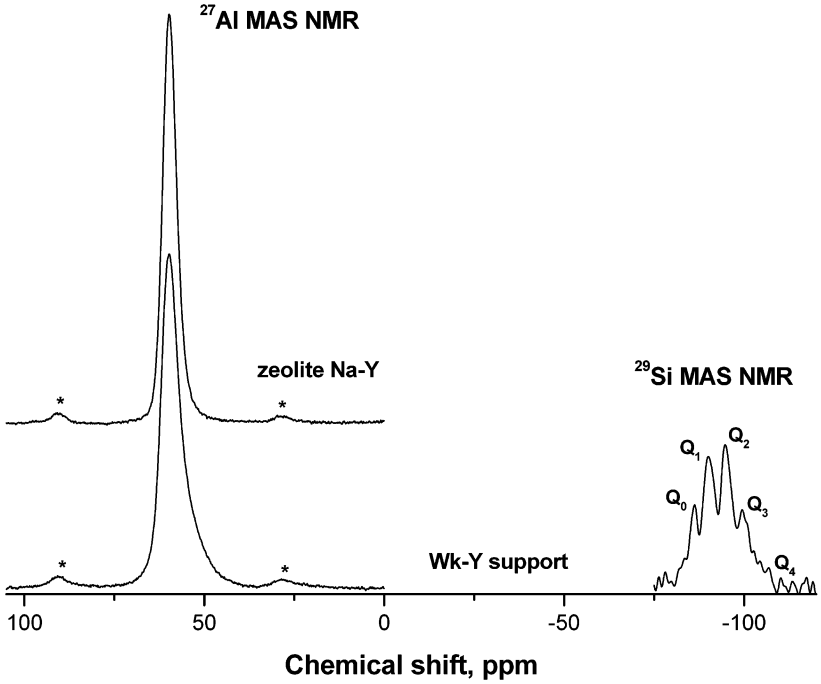

Figure 2. ^{27}Al and ^{29}Si MAS NMR spectra of zeolite Na−Y and Wk−Y supports (* in NMR patterns denote sidebands at 4 kHz).

which probably are due to ν_{Rh-NH2} frequency; of course, an overlap of this band with that of the untethered surface silanol groups (ν_{OH}) lying in the same frequency range is also not overruled.

(c) ^{29}Si and ^{27}Al MAS NMR Spectra of the Encapsulated Catalysts. ^{29}Si and ^{27}Al MAS NMR spectra (at 99.44 and 130.42 MHz, respectively, at 11.7 T) of Wk−Y confirmed that the framework Si/Al ratio[15] remains the same (2.37) as that of zeolite Na−Y used here, thus showing that the framework structure is intact after encapsulation (Figure 2). In the ^{29}Si MAS NMR spectra of Wk−Y, Q^4 (nAl wherein $n = 0, 1, 2, 3$) environments were detected in Na−Y as well as in Wk−Y, further suggesting that the Al site distributions and population remain unaltered. The ^{27}Al MAS NMR in case of Wk−Y confirms that all Al or most of the Al atoms were in the tetrahedral framework environment and not replaced by Rh atoms (Figure 2).

^{29}Si MAS NMR spectra of Wk-M41 and Wk-M48 (spectra not shown) revealed almost no variations in the Q^3 ($(SiO)_3{\equiv}Si-OH$) and Q^4 ($(SiO)_3{\equiv}Si-O-Si{\equiv}$) chemical shifts ($\delta = -100$ ppm and -110 ppm respectively) although, there was a substantial change observed in the Q^3/Q^4 ratio (Table 1). A possible reason for the lower Q^3/Q^4 values might be the decrease in population of the free silanol groups of the Q^3 species due to the linkage arising from anchoring of APTS with the silanol groups (of the Q^3 species) present in the mesoporous materials. This further confirmed that the mesostructures of Wk-M41 and Wk-M48 were intact even after encapsulation of the Rh complex in the mesoporous materials.

(d) X-ray Photoelectron Spectra (XPS) of the Encapsulated Catalysts. XPS of the samples were recorded in a VG Microtech ESCA 3000 spectrometer, using unmonochromatized Mg K_α (-1253.6 eV) as the radiation source, applying vacuum at 10^{-10} Torr and pass energy of 50 eV. Surface analysis by XPS spectra was carried out in terms of the binding energy (BE) values of various elements present in the catalyst supports after necessary C1s correction, especially taking into consideration the Rh $3d_{5/2}$ and $3d_{3/2}$ BE values for catalysts Wk−Y, Wk-M41, and Wk-M48 (Figure 3). XPS of these catalysts were also performed after hydroformylation reactions in order to record any change observed in the oxidation states or BE values of the elements present in the supports during the reaction, and these were found to be in compliance with the literature values.[16] The BE values of the supports before and after hydroformylation reactions were almost similar, which proves essentially that all rhodium was present as Rh(I) in the encapsulated materials and the oxidation state remained unaltered even after reactions (Table 2). The silicon, phosphorus, rhodium(I), aluminum (in Wk−Y) and nitrogen (in Wk-M41 and Wk-M48) present in various supports showed no change in their BE values. A slight decrease in BE values of rhodium(I) (by 1 eV) was observed for Wk−Y in contrast to Wk-M41 or Wk-M48. This might be due to the different immobilization procedures used for $HRh(CO)(PPh_3)_3$ encapsulation inside the pores of zeolite Na−Y and mesoporous MCM-41 and MCM-48 materials. During the synthesis of catalyst Wk−Y, the encapsulation of $HRh(CO)(PPh_3)_3$ might have caused removal of some of the sodium cations from the zeolitic sites to place the complex in the supercage by a "ship-in-a-bottle" fashion. In the case

(15) (a) Engelhardt, G.; Michel, D. *High-Resolution Solid-State NMR of Silicates and Zeolites*; Wiley: New York, 1987; pp 150−228. (b) Fyfe, C. A.; Thomas, J. M.; Klinowski, J.; Gobbi, G. C. *Angew. Chem., Int. Ed. Engl.* **1983**, *22*, 259. The Si/Al ratio in the tetrahedral alumonosilicate framework was calculated after deconvolution (using Jandel Scientific Peakfit program) from the equation

$$(Si/Al)_{NMR} = \Sigma_{n=0}^{4} I_{Si(nAl)} / \Sigma_{n=0}^{4} 0.25 n I_{Si(nAl)}$$

(16) (a) Wagner, C. D., Riggs, W. M., Davis, L. E., Moulder, J. E., Muilenberg, Eds.; *Handbook of X-ray Photoelectron Spectroscopy*; Perkin-Elmer Corporation: Wellesley, MA, 1979. (b) Andersson, S. L. T.; Scurrell, M. S. *J. Catal.* **1979**, *59*, 340.

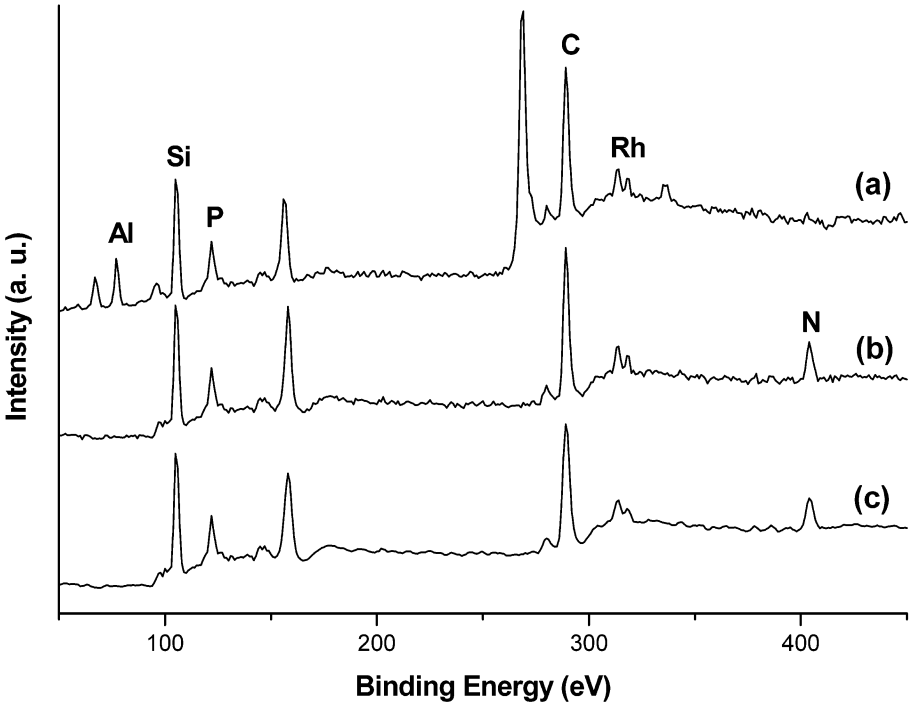

Figure 3. X-ray photoelectron spectra of (a) Wk−Y, (b) Wk-M41, and (c) Wk-M48 supports.

Table 2. XPS Binding Energy Values[a] for Different Elements Present in Various Encapsulated Catalysts Before (B) and After (A) Hydroformylation of Styrene

	Element				
support	Al	Si	P	Rh ($3d_{5/2}$, $3d_{3/2}$)	N
Wk−Y−B	74.8	102.7	126.9	310.2, 314.8	
Wk−Y−A	74.7	102.8	127.0	310.3, 314.8	
Wk-M41-B		103.3	127.2	309.3, 313.8	400.2
Wk-M41-A		103.3	127.3	309.6, 314.0	400.1
Wk-M48-B		103.3	127.1	309.5, 314.1	400.1
Wk-M48-A		103.3	127.2	309.7, 314.2	400.1

[a] All the values were corrected to C 1s with binding energy of 285 eV using adventitious carbon.

of Wk-M41 and Wk-M48 catalysts, the Rh complex was anchored inside the mesopores' walls by tethering to amino groups bonded to the silica matrixes. In the latter case (the mesoporous systems), we presume that an ionic interaction rather than a covalent one accounted for the decrease in rhodium(I) binding energy values (BE values of Rh $3d_{5/2}$: 310.2, 309.3, and 309.5 for Wk−Y, Wk-M41, and Wk-M48, respectively). This further showed that the integrity of the $HRh(CO)(PPh_3)_3$ complex was retained when encapsulated in the supports and that all the rhodium was present as Rh(I) with no beam damage suffered by the encapsulated supports.

(e) Powder X-ray Diffraction (XRD) Patterns of the Encapsulated Catalysts. Powder XRD of the encapsulated catalysts and supports were obtained at room temperature on a Rigaku D MAX III VC diffractometer using Ni-filtered Cu Kα radiation, $\lambda = 1.5404$ Å. In the case of MCM-41, MCM-48, Wk-M41, and Wk-M48, observable 2θ ranges were from 1.5° and 10° at a scan rate of 1°/min, whereas in the case of zeolite Na−Y and Wk−Y, observable 2θ ranges were from 5° and 50° at a scan rate of 8°/min. A comparison of the bare supports (Na−Y, MCM-41, and MCM-48) and $HRh(CO)(PPh_3)_3$ encapsulated catalysts (Wk−Y, Wk-M41, and Wk-M48) by powder XRD has been presented in Table 1 and Figure 4. This showed that the respective cubic (*Ia*3*d*) and hexagonal (*p*6*mm*) mesoporous phases of MCM-48, Wk-M48, MCM-41, and Wk-M41 remain unaltered in peak positions. The changes in respective intensities have been observed perhaps due to pore fillings of the $HRh(CO)(PPh_3)_3$ complex inside mesopores. Distinct Bragg reflections at {100}, {110}, {200}, and {210} for MCM-41 and Wk-M41 (Figure 4a,b) and at {211}, {220}, {321}, {400}, {420}, {332}, {422}, and {431} for MCM-48 and Wk-M48 (Figure 4c,d), further confirmed the restoration of the respective ordered patterns of the bare and the Rh-complex-encapsulated mesoporous matrixes without any breakdown of the mesostructures. In case of zeolite Na−Y and its impregnated and encapsulated analogues (Wk−Y−S and Wk−Y respectively), retention of the microporous phase zeolite Y was confirmed, though differences in the peak intensities were observed in case of Wk−Y sample (Figure 4e−g). Earlier, with the aid of powder XRD, Quayle et al.[17] reported an empirically derived relationship as a possible explanation for the encapsulation of Fe(II) and Ru(II) complexes inside zeolite Y by a term $I_{331} > I_{311} > I_{220}$ (where I represents intensity). In our case however, we have not observed any such patterns, probably due to differences in the encapsulation procedure (of the Rh complex entrapped in zeolite Y). In contrast, we observed a marked decrease in the intensity of {111} diffraction pattern of Wk−Y as compared to that of Na−Y or Wk−Y−S (Figure 4e−g), which showed almost no difference in the peak intensities owing to random distribution of cations (due to impregnation) within the zeolite lattice (wherein $I_{331} > I_{220} > I_{311}$). We presume that the noticeable decrease in the {111} intensity of the Wk−Y sample might have occurred due to possible incorporation of $HRh(CO)(PPh_3)_3$ complex inside the framework

(17) (a) Quayle, W. H.; Lunsford, J. H. *Inorg. Chem.* **1982**, *21*, 97. (b) Quayle, W. H.; Peeters, G.; De Roy, G. L.; Vansant, E. F.; Lunsford, J. H. *ibid.* 2226.

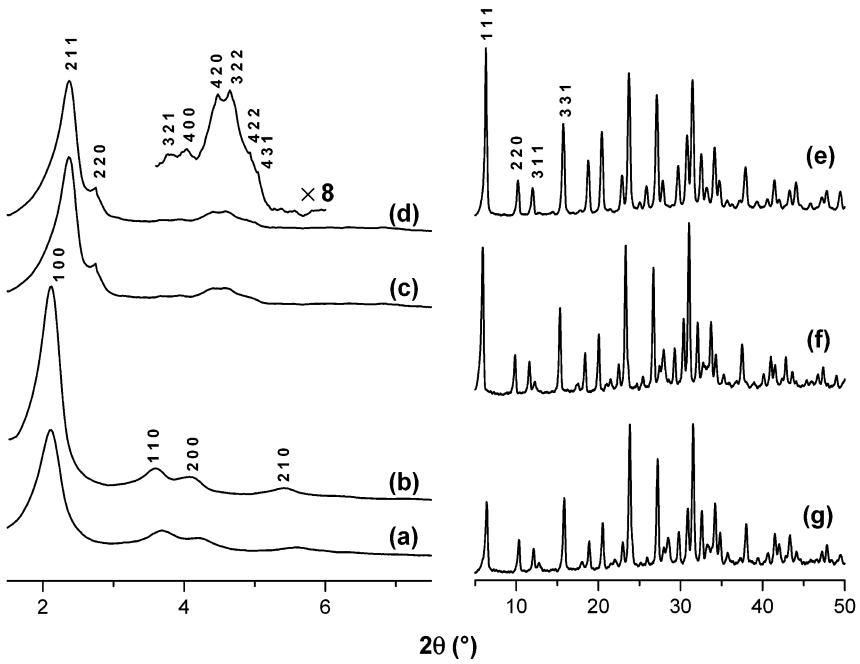

Figure 4. Powder X-ray diffraction patterns of (a) Wk-M41, (b) MCM-41, (c) Wk-M48, (d) MCM-48, (e) Na−Y, (f) Wk−Y (supported), and (g) Wk−Y (encapsulated).

of zeolite Y. But it was confirmed by XRD that the porous framework of encapsulated supports (microporous as well as mesoporous) was not affected or damaged during the Rh complex entrapment.

(f) Transmission Electron Microscopy (TEM) of the Encapsulated Catalysts. TEM has been used extensively for structural elucidation of zeolites and mesoporous materials.[5,18] Recently, to envisage three-dimensional structures of micro- and mesoporous solids, imaging nanoparticle catalysts inside mesoporous hosts and determine their occluded structure-directing organic species, high-resolution TEM was used as a convincing tool.[6b,19] To direct the location of the anchored Rh complex inside the pores, we imaged the mesoporous MCM-41 and MCM-48, Ph_2SiCl_2–untreated Wk-M41−S and Wk-M48−S, microporous Na−Y, and their encapsulated analogues (Wk-M41, Wk-M48, and Wk−Y) by TEM (Figure 5). The samples were dispersed in 2-propanol and placed on holey carbon grids, and a JEOL model 1200 EX instrument operated at an accelerating voltage of 100 kV was used for imaging the samples. The TEM images of bare MCM-41 and MCM-48 were consistent with the regular hexagonal and cubic mesophases, respectively, (Figure 5a,c (insets)) with homogeneity in patterns throughout.

TEM images of Wk-M41−S and Wk-M48−S (Figure 5a,c) indicate the presence of Rh complex tethered by APTS (by a host−guest interaction) at the external surfaces of MCM-41 and MCM-48. In contrast, startling differences in the TEM images were observed when these images were compared with the Wk-M41 and Wk-M48 samples (Figure 5b,d), wherein the Rh complex has been encapsulated exclusively inside the mesopores by treating with Ph_2SiCl_2. A comparison of the images of Wk-M41−S and Wk-M48−S (Figures 5a,c) with those of Wk-M41 and Wk-M48 (Figure 5b,d) showed "clean" exterior surfaces of the latter ones with retention of strong image contrasts of the grafted Rh complex inside the mesopores. The encapsulated samples prepared by treating with Ph_2SiCl_2 and further tethered with APTS, established that the Rh complex is immobilized totally inside the mesopores and the distribution of the complex entrapped inside was very much uniform, unlike Wk-M41−S and Wk-M48−S materials (untreated with Ph_2SiCl_2, Rh complex bound to the external mesopores' walls); a similar fact was observed by Shephard et al.[6b] earlier. Thus, by TEM we could not only image the hexagonal and cubic patterns of the mesoporous materials, but also distinctly distinguish the internally bound Rh complex from the externally grafted ones.

In another survey, TEM was used to image the diffraction patterns of zeolite Na−Y and Wk−Y (Figure 5e,f). We could observe another distinction between the bare and the encapsulated samples, wherein the "neat" zeolite Y showed well-resolved cubic diffraction patterns, whereas Wk−Y showed a "foggy" image. In Wk−Y, the encapsulated Rh complex occupying the faujasite supercage obscures the zeolite pores, hence, the "foggy" diffraction pattern is observed. This might be a possible reason for obtaining decreased {111}-diffraction intensity in the XRD patterns of Wk−Y as we had observed earlier (Figure 4).

These characterizations supported the absence of the complex at the solid surface with no noticeable Rh clusters and restoration of the uniformity of the catalysts. For a better understanding, we investigated for the clue to an obvious question: whether the Rh complex with three bulky PPh_3 groups is able to sit inside the supercage of zeolite Y without any conformation change or bond breakage. An insight into the crystal structure of $HRh(CO)(PPh_3)_3$[14a,b] reveals that the

(18) Bursill, L. A.; Lodge, E. A.; Thomas, J. M. *Nature* **1980**, *286*, 111.

(19) (a) Thomas, J. M.; Terasaki, O.; Gai, P. L.; Zhou, W. Z.; Gonzalez-Calbet, J. *Acc. Chem. Res.* **2001**, *34*, 583. (b) Ozkaya, D.; Zhou, W. Z., Thomas, J. M.; Midgley, P. A.; Keast, V. J.; Hermans, S. *Catal. Lett.* **1999**, *60*, 113.

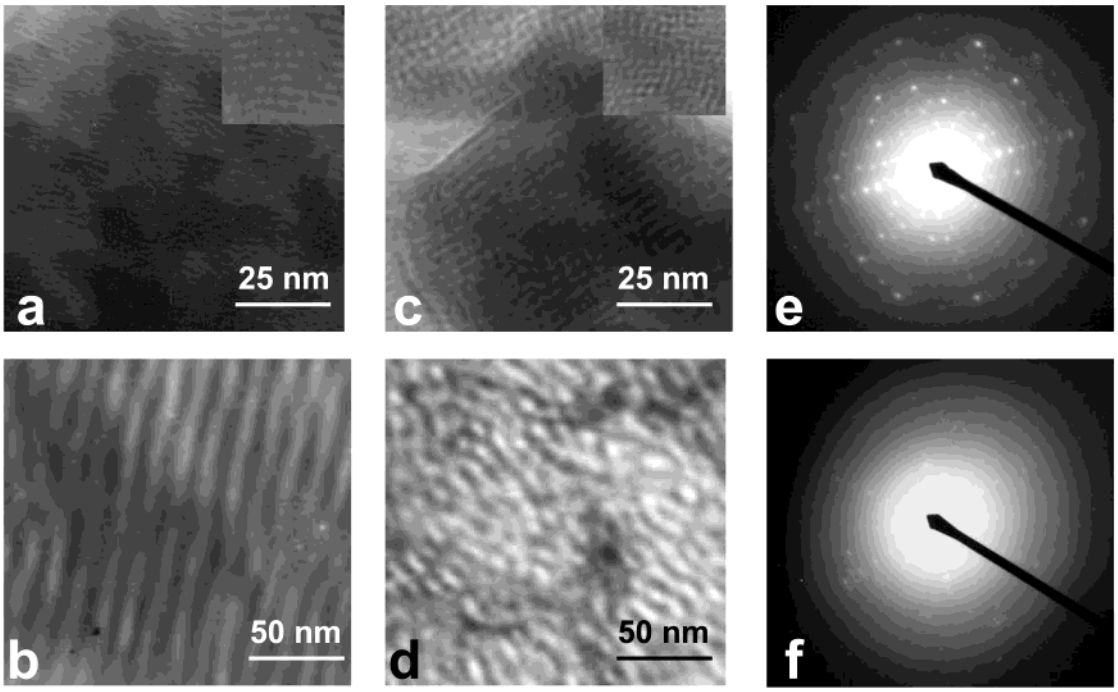

Figure 5. TEM images of (a) Wk-M41−S (untreated with Ph_2SiCl_2), inset: MCM-41; (b) Wk-M41 (treated with Ph_2SiCl_2), inset: MCM-48; (c) Wk-M48−S (untreated with Ph_2SiCl_2); (d) Wk-M48 (untreated with Ph_2SiCl_2); (e) diffraction patterns of Na−Y; and (f) diffraction patterns of Wk−Y.

dimension of the complex is close to 10.8 × 10.7 × 10.8 (Å)^3. This reflects that entrapment of $HRh(CO(PPh_3)_3$ inside the zeolite Y supercage (12−13 Å) is very much feasible (since we prepare Wk−Y by a "ship-in-a-bottle" approach[20]), while there are no doubts for ∼30 Å mesopores of MCM-41 and MCM-48 to accommodate the Rh complex inside. Thus, on the basis of our characterizations and observations, we can conclude that $HRh(CO)(PPh_3)_3$ is encapsulated in the zeolite Y supercage and MCM-41 and MCM-48 mesopores (Figure 6 top, bottom) and not merely impregnated/adhered on the porous surface.

2. Performance of the Encapsulated Catalysts for Hydroformylation of Olefins. The hydroformylation reaction products were analyzed by gas chromatograph (GC) on a Hewlett-Packard machine (HP 5890) fitted with an HP 5 capillary column and ^{1}H NMR. The heterogeneous catalysts before and after reactions were also characterized by inductively coupled plasma spectrophotometer (ICP; Perkin-Elmer 1200) for the elemental analysis of rhodium to assess metal leaching in the course of reaction.

The catalysts Wk−Y, Wk-M41, and Wk-M48 were evaluated for their activity and selectivity behavior for hydroformylation of 1-octene (Table 3, entries 10−12) and styrene (Table 4). Particularly, it is shown that these encapsulated rhodium complex catalysts are highly stable, can be recycled several times (each catalyst was recycled 10 times) without losing activity or selectivity, and do not require presence of free PPh_3 as a ligand. These catalysts (Table 3, entries 10−12), when compared to the other previously reported heterogeneous catalysts for hydroformylation, exhibit superior activity, recyclability, and selectivity. For the Rh−SiO_2 immobilized catalysts (Table 3, entries 7−9), though the *n*/iso ratio for *n*-nonaldehyde is significantly higher than that of our catalysts (Table 3, entries 10−12), TOF values are lower, and in one case metal leaching (>50%) was observed (Table 3, entry 9) which is undesirable for a true heterogeneous catalyst. With all three encapsulated catalyst systems, high conversion (>97%) and selectivity toward aldehydes (>98%) were obtained (Table 4). The selectivity toward the desirable products was found to be comparable for styrene and 1-hexene, but lower for higher olefinic substrates (1-octene, 1-decene, 1-dodecene) in almost all the cases. A plausible reason might be the geometric constraints of the substrates accessing the complex site inside the pores. The enhanced activity for Wk-M41 and Wk-M48 is due to larger pore dimensions in these catalysts (∼30 Å) that give better access for the substrates to the catalytic sites present inside the mesopores of MCM-48, in comparison to that of confined micropores of zeolite Y having a 12 Å supercage and an 8 Å window.

In a typical experiment using Wk-M48−S catalyst (Rh content 0.63 wt/wt %) for hydroformylation of styrene, we observed ∼6% overall Rh leaching, compared to <0.05% overall Rh leaching using Wk-M48 catalyst (Rh content 0.69 wt/wt %) after 6 recycles. Therefore, this method (Ph_2SiCl_2 treatment with the mesoporous materials) coupled with anchoring of APTS and Rh complex inside the mesopores provides a distinct advantage over the conventional anchoring method with APTS (no Ph_2SiCl_2 treatment) in avoiding Rh leaching in the course

(20) For an excellent review on this topic we refer the reader to (a) De Vos, D. E.; Thibault-Starzyk, F.; Knops-Gerrits, P. P.; Parton, R. F.; Jacobs, P. A. *Macromol. Symp.* **1994**, *80*, 157. (b) Herron, N. *Inorg. Chem.* **1986**, *25*, 4741.

(21) The specific surface areas of the samples were determined by the BET method using N_2 adsorption measured with an Omnisorb CX-100 Coulter instrument. Prior to the adsorption, the samples were activated at 150 °C for 6 h at 10^{-4} Torr. Particles were imaged by Scanning Electron Microscope (Philips model XL 30). Q^3/Q^4 values obtained from ^{29}Si MAS NMR spectra of the as-synthesized and calcined sample determined after deconvolution of Q^3 and Q^4 peaks by Jandel Scientific Peakfit program.

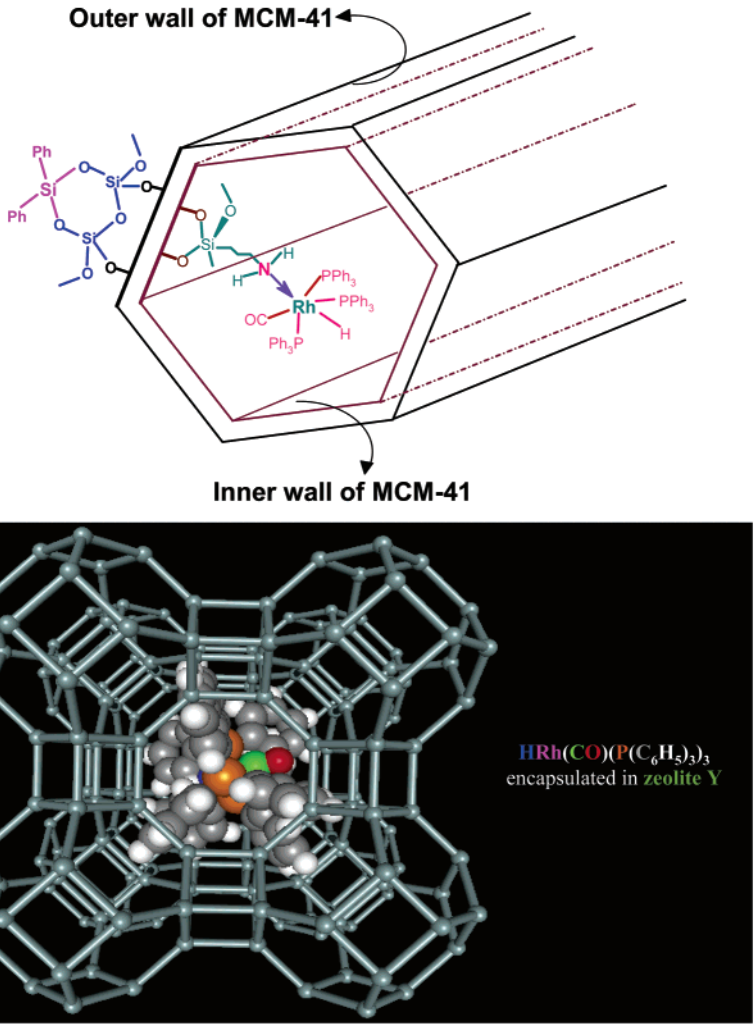

Figure 6. (top) Model of $HRh(CO)(PPh_3)_3$ complex anchored inside the inner wall of MCM-41 channel by 3-aminopropyltrimethoxysilane, and outer wall of the MCM-41 channel derivatized by dichlorodiphenylsilane. (bottom) Molecular model representation of Wk−Y (structure generated in an Indigo II machine using Insight II software).

Table 3. Comparison Activity and Selectivity of Few Selected Heterogeneous Catalysts Used in Hydroformylation of Various Olefins

entry	substrate	S/ Rh[a]	conv.[b] (%)	n/iso	TON	TOF (h^{-1})	Rh leaching, %	catalyst used[c]	reference
1	1-hexene	100	37.0	2.3	37.0	1.7	trace	Rh−Y	10 (b)
2	1-hexene	100	88.5	0.6	88.5	29.5	n. d.	Rh−SiO_2	10 (g)
3	1-pentene	106	97.1	2.7	103.0	22.9	appreciable	Rh−polymer	9 (a)
4	1-decene	200	81.0	1.5	162.0	40.5	appreciable	Rh_2−MCM-41	9 (h)
5[d]	oleyl alcohol	500	96.6	n. d.	483.0	87.8	untraced	Rh−SAPC 9	9 (c)
6	1-octene	250	75.0	2.6	187.5	7.8	untraced	Rh−calix[4]arene	10 (d)
7[e]	1-octene	4255	9.4	32.0	400.0	87.0	untraced	Rh−$ScCO_2$	10 (f)
8	1-octene	637	69.0	32.0	440.0	35.0	< 1	Rh−SiO_2	10 (e)
9[f]	1-octene	637	64.0	1.6	408.0	175.0	> 50	Rh−SiO_2	10 (e)
10[g]	1-octene	581	97.2	1.5	565.0	141.0	< 0.01	Rh−Y	Wk−Y
11[g]	1-octene	879	98.2	1.7	863.0	216.0	< 0.01	Rh−MCM-41	Wk-M41
12[g]	1-octene	951	99.4	1.7	945.0	270.0	< 0.01	Rh−MCM-48	Wk-M48

[a] S/Rh = substrate/rhodium ratio. [b] Conversion to aldehydes. [c] The term Rh has been used for various Rh-complexes used as catalysts. [d] Supported aqueous phase catalyst. [e] Supercritical conditions, 180 bar CO_2, reaction temperature 353 K. [f] Without addition of free ligand. [g] Rh-leached (%) after single run, see Table 4 for reaction conditions; TON = kmol of olefins converted to aldehydes × (kmol of Rh)$^{-1}$; TOF = TON × h^{-1}; n. d. = not determined.

of reaction due to prolonged use. Using impregnated Rh complex on zeolite Y (Wk−Y−S) showed higher activity due to appreciable leaching of Rh metal from the support (~27% Rh loss in a single run; Table 4). Hence, true heterogeneity in case of encapsulated catalysts (Wk−Y, Wk-M41, and Wk-M48) could be established in comparison to the impregnated Wk−Y−S or untreated Ph_2SiCl_2 catalysts (Wk-M41−S and Wk-M48−S). Because Wk-M48 showed the best activity and selectivity for styrene hydroformylation among the heterogeneous catalysts used (Table 4), it was selected for further work on comparison of its activity and selectivity with that of homogeneous $HRh(CO)(PPh_3)_3$ catalyst for hydroformylation of olefins (Table 5). Though the TONs and TOFs for the heterogeneous catalysts were lower than those for the homogeneous $HRh(CO)(PPh_3)_3$ catalyst,

Table 4. Activity and Selectivity of Hydroformylation of Styrene Using Various Catalysts[a]

entry	catalyst	conversion (%)	selectivity ald. (%)	*n*/iso	Rh content (wt/wt %)	% Rh leaching [b]	TON	TOF (h^{-1})	time (h)
1	Wk−Y	100	98.1	0.67	1.130	0.053[c]	780	173	4.5
2	Wk−Y−S	99	98.5	0.44	0.567	∼ 27.0	1700	567	3.0
3	Wk-M41	100	99.1	0.43	0.747	0.054[c]	1200	279	4.3
4	Wk-M48	100	99.1	0.43	0.690	0.043[c]	1300	325	4.0
5	Wk-M48−S	99	99.0	0.41	0.630	∼ 6.0 [c]	1750	583	3.0
6	$HRh(CO)(PPh_3)_3$	98	98.9	0.33	11.21		2675	2876	0.93

[a] Reaction conditions: catalyst, 8 kg m^{-3} for entries 1−5 and 0.96 kg m^{-3} for entry 6; substrate, 0.698 kmol m^{-3} for entries 1−5 and 3.49 kmol m^{-3} for entry 6; P_{CO}, P_{H2}, 2.04 MPa; agitation speed, 16.67 Hz; temperature, 373 K; solvent, toluene; total volume, 2.5×10^{-5} m^3; TON = kmol of styrene converted to aldehydes × (kmol of Rh)$^{-1}$; TOF = TON × h^{-1}. [b] Rh-leaching (%) = ppm of Rh-leached × 100/ppm of Rh-content (evaluated from Rh-content wt/wt %). [c] Overall Rh-leached after 6 recycles, otherwise, for single run.

Table 5. Comparison of Activity and Selectivity of Hydroformylation of Linear Olefins Using $HRh(CO)(PPh_3)_3$ and Wk-M48 Catalysts[a]

entry	catalysts	substrate	substrate (kmol m^{-3})	conversion (%)	selectivity ald. (%)	*n*/iso	TON	TOF (h^{-1})	time (h)
1	$HRh(CO)(PPh_3)_3$	1-hexene	3.198	98.8	98.8	2.55	2450	2467	1.05
2	Wk-M48	1-hexene	0.639	100.0	99.5	2.33	1182	338	3.50
3	$HRh(CO)(PPh_3)_3$	1-octene	2.548	98.8	98.2	2.42	1850	1391	1.33
4	Wk-M48	1-octene	0.509	100.0	99.4	1.67	945	270	3.50
5	$HRh(CO)(PPh_3)_3$	1-decene	2.113	98.2	92.2	1.36	1518	961	1.58
6	Wk-M48	1-decene	0.423	99.0	99.2	1.50	383	109	3.50
7	$HRh(CO)(PPh_3)_3$	1-dodecene	1.801	97.4	89.1	0.79	1210	630	1.92
8	Wk-M48	1-dodecene	0.360	99.0	98.6	1.00	326	88	3.70

[a] Reaction conditions: catalyst, 0.96 kg m^{-3} $HRh(CO)(PPh_3)_3$ and 8 kg m^{-3} Wk-M48 (0.69 wt/wt % Rh); P_{CO}, P_{H2}, 2.04 MPa; agitation speed, 16.67 Hz; temperature, 373 K; solvent, toluene; total volume, 2.5×10^{-5} m^3; TON = kmol of olefin converted to aldehydes × (kmol of Rh)$^{-1}$; TOF = TON × h^{-1}.

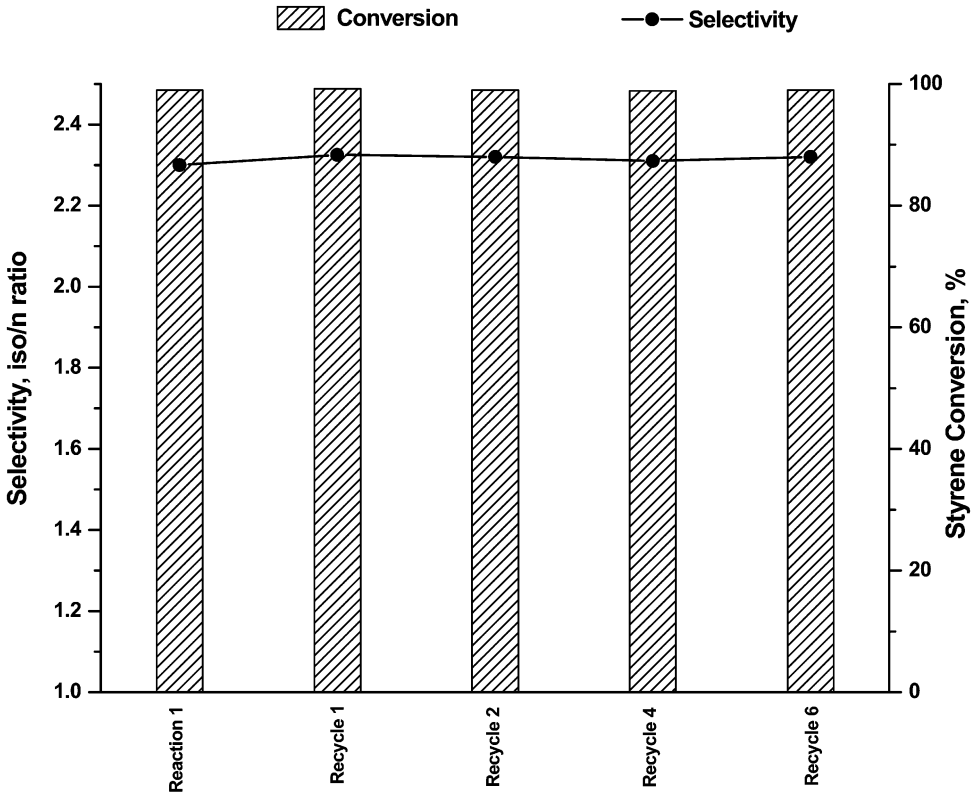

Figure 7. Recycle studies using Wk-M48 catalyst for hydroformylation of styrene.

the encapsulated catalysts could be easily separated from the reaction mixtures and recycled several times, an obvious advantage over the homogeneous catalyst.

A typical recycle experiment with Wk-M48 catalyst for hydroformylation of styrene showed that the catalyst is truly stable even after 6 recycles without loosing activity or selectivity (Figure 7). Elemental analysis for Rh of these encapsulated catalysts, as well as of the reaction mixtures before and after the reaction by ICP, showed <0.05% overall Rh loss after the 6th recycle, thus ensuring negligible leaching of rhodium from the catalyst. The reaction mixture, after separation of the solid catalyst, was also tested for hydroformylation activity (after catalyst removal from the 5th recycle); it showed no catalytic activity (Rh content was below detection limit of the ICP-AES instrument, 0.01 ppm),

further supporting that the leaching of Rh from the catalyst was negligible.

Conclusions

We describe here novel heterogeneous catalysts consisting of encapsulated $HRh(CO)(PPh_3)_3$ in the pores of microporous Na−Y, cubic MCM-48, and hexagonal MCM-41 materials, for hydroformylation of olefins. The use of such air-stable catalysts showed high activity, recyclability, and easy catalyst−product separation from the liquid phase, though the *n*/iso ratio was lower when compared to that of the homogeneous catalyst $HRh(CO)(PPh_3)_3$. Though the reaction rates were lower than those of the homogeneous system, the cumulative turnover numbers for the encapsulated catalysts were significantly higher considering recycle experiments with complete conversion of olefins in each batch cycle. These encapsulated catalysts can open up new vistas for the industrial applications in synthesis of high boiling specialty aldehydes. This approach can also be extended to encapsulate Rh complexes with other ligands to tailor the desired *n*/iso selectivity in specific cases.

Acknowledgment. K.M. thanks the Council of Scientific and Industrial Research (CSIR), New Delhi, for a fellowship. We thank immensely Dr. S. Ganapathy, Dr. P. Rajamohanan, and Mr. K. Damodaran for their help in recording the NMR spectra and valuable discussions, Mr. A. Ghosh for recording the XRD spectra, and Ms. R. Parischa for TEM.

CM020752N